Journal of Alloys and Compounds 506 (2010) 902–912

Contents lists available at ScienceDirect

Journal of Alloys and Compounds

journal homepage: www.elsevier.com/locate/jallcom

Preparation and characterization of proton conducting phosphosilicate glass membranes with different catalyst layers for low-temperature H_2/O_2 fuel cells

K. Tanaka, G. Lakshminarayana, Randy Jalem, Masayuki Nogami*

Department of Materials Science and Engineering, Nagoya Institute of Technology, Showa, Nagoya 466-8555, Japan

ARTICLE INFO

Article history:
Received 5 September 2009
Accepted 14 July 2010
Available online 22 July 2010

Keywords:
H_2/O_2 fuel cell
Glass membrane
Electrolyte
Proton conductivity

ABSTRACT

In this paper, we report on the proton conducting phosphosilicate glass membranes using TiO_2, Pt, and Nafion® as intermediate layers, respectively, for their applicability as low-temperature fuel cells electrolytes. Measurements concerning Scanning Electron Microscopy (SEM), Electrochemical Impedance Spectroscopy (EIS), as well as electrochemical analysis were carried out. The specific surface area and pore size distributions were described by the Brunauer–Emmett–Teller (BET) method and the average pore size found to be approximately in the range of 2.8–6.3 nm for all the studied membranes. The electric current–voltage characteristics of the fabricated MEA were studied under humidified atmosphere. When electrode width is 4 or 9 mm, the obtained maximum current and power density values are 147.1 mA cm^2 and 73.8 mW cm^2; and 68.2 mA cm^2 and 27.2 mW cm^2, respectively. It is thought that the catalyst reaction efficiency in three-phase boundary improved and higher output power can be obtained with the electrodes used. In addition with high output values, internal resistance is also decreased due to small width of electrode. Thus the studied membranes are suitable candidates for low-temperature H_2/O_2 fuel cells electrolytes.

1. Introduction

Fuel cells are attractive for use in transport and stationary applications for a variety of reasons, such as high energy density, low cost, easy transportation, and low reforming temperature. Also, fuel cells are believed to find their first widespread use in portable electronics. The H_2/O_2 fuel cells are very efficient devices for the conversion of chemical energy into electrical energy. Additional research is vitally needed to understand and evaluate the best potential uses of fuel cells in transportation and mobile applications. The development of effective and low cost membranes for fuel cells has gained fundamental importance and turned out to be a challenge for the membrane community in the last years [1–7]. The challenge particularly consists in fabricating low cost membranes out of glass for low-temperature H_2/O_2 fuel cells. Low-temperature fuel cells, in particular proton exchange membrane (PEM) fuel cells, are the most suited for transport applications since there are no problems with temperature cycling. The glass membranes play a decisive role as electrolyte media for proton transport and barriers to avoid the direct contact between the fuel and oxygen. The low operating temperatures will allow for an easier cell construction, enabling cheaper materials to be used, and will reduce the problem of thermal stress. A good proton conducting electrolyte should combine high chemical, mechanical, and thermal stabilities with reasonable electrochemical properties [8–11].

Phosphosilicate glasses exhibit interesting technological and structural properties. In particular, they find uses in energy generating applications, such as hydrogen fuel cells and proton exchange membrane fuel cells, because of their ability to act as fast proton conductors [12–14]. The POH bonds, strongly hydrogen-bonded with water molecules, are appropriate for increasing the proton conduction, while the SiO_2 is useful to increase the mechanical strength of the glass. The conductivity also increases with increasing water content in the pores. Although these materials can be prepared by a conventional ceramic route, sol–gel synthetic methods are a viable alternative not only because they represent a lower cost technology but also because better mixing of the starting materials can be achieved on the molecular scale. Recently, from our laboratory the preparation of porous SiO_2–P_2O_5 glasses, which displayed a conductivity of $\sim 10^{-2}$ S/cm at room temperature [1,15,16], were reported. These glasses were applied to the electrolyte of hydrogen/oxygen fuel cell, exhibiting power densities of order of $\sim$10 mW/cm^2 at room temperature. In the present work, proton conducting phosphosilicate glass membranes mixed with TiO_2, Pt, and Nafion® as intermediate layers, respectively, are being designed and developed for a systematic study. Such membranes are expected to possess high proton conductivities under humidified conditions at room temperature and high

* Corresponding author. Tel.: +81 52 735 5285; fax: +81 52 735 5285.
E-mail address: nogami@nitech.ac.jp (M. Nogami).

0925-8388/$ – see front matter © 2010 Elsevier B.V. All rights reserved.
doi:10.1016/j.jallcom.2010.07.113

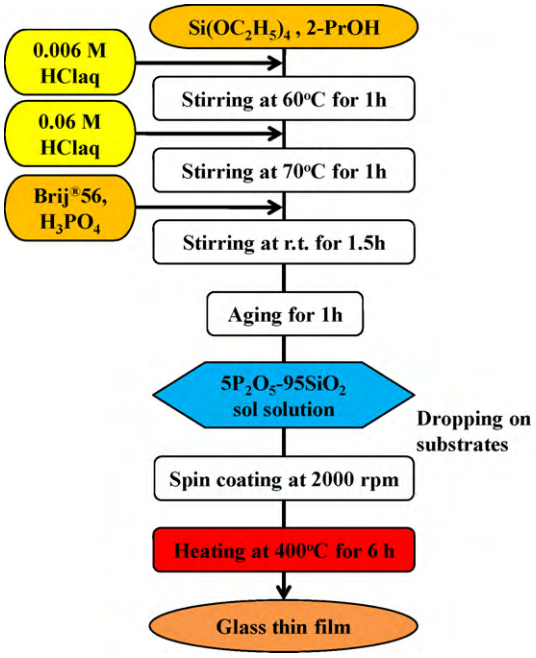

Fig. 1. Flowchart for the sol–gel synthesis of $5P_2O_5$–$95SiO_2$ glass thin film.

thermal, mechanical, chemical, and electrochemical stabilities. To achieve these targets, the prepared SiO_2–P_2O_5 glass membranes were characterized by various experimental techniques, i.e., Scanning Electron Microscopy (SEM), Electrochemical Impedance Spectroscopy (EIS), as well as electrochemical analysis including H_2/O_2 fuel cell test.

2. Experimental studies

Fig. 1 shows the procedure followed for the preparation of the phosphosilicate glass thin film. The precursors used were Si $(OC_2H_5)_4$ (TEOS) and H_3PO_4. The glass composition was set to be $5P_2O_5$–$95SiO_2$ (mol%). First, 6.0×10^{-3} M HCl aqueous solution was slowly added to the C_3H_8OH (2-PrOH) and TEOS mixed solution, stirred at 60 °C to obtain partially hydrolyzed solution. In order to increase hydrolysis, 6.0×10^{-2} M HCl aqueous solution was also added drop-wise and then stirred vigorously at 70 °C. After that, Brij®56 and H_3PO_4 were added and the solution was again stirred for another 1.5 h. Stirring was then stopped and the final solution was aged for 1 h. The mole proportion was TEOS:2-PrOH:H_2O:HCl:Brij®56 = 1:x:5:5×10^{-3}:0.1 (x = 3, 4, 5, 7, 10, 15). The ratio of C_3H_8OH (2-PrOH) and TEOS was changed. A slide glass (Matsunami Co.) was used as a substrate for the conductivity measurement. ITO glass (Asahi Glass Co., Ltd.) was coated with Pt by vapor deposition. Vycor glass (Coning Co.) was used for current/voltage characteristics measurement. The prepared sol with a volume of 100 μl was then spin-coated at 2000 rpm for 90 s. The coating was then allowed to dry in air. The coated substrate was heated in an electric furnace. The heating temperature was set to 400 °C and the keeping time was 6 h.

3. Results and discussion

Fig. 2 shows the relationship between the mol ratio of 2-PrOH for TEOS and film thickness of the glass. The proportion TEOS:2-PrOH = 1:x (mol%), with x = 3, 4, 5, 7, 10, 15, resulted in film thickness of 1000, 750, 620, 440, 300 and 170 nm, respectively. With the decrease of 2-PrOH, film thickness increased. At low speed spin coating, film thickness is also increased due to highly viscous sol. Noting that the rotation speed was fixed at 2000 rpm, the decrease in 2-PrOH led to an increase in sol viscosity thereby causing the film thickness to increase. From this fact, the quantity of the solvent can be adjusted to obtain the glass thin film with desired thickness. Fig. 3 shows the prepared $5P_2O_5$–$95SiO_2$ glass thin film (TEOS:2-PrOH = 1:3) pore size distribution. The average pore diameter was determined to be about 2.8 nm with Brij®56 as the ionic surfactant. Table 1 shows the pore characteristics of the glass thin film. Fig. 4 shows the adsorption–desorption isotherm of the $5P_2O_5$–$95SiO_2$ glass thin film. Equilibrium was attained at the part with low relative pressure at P/P_0 = 0.3 as indicated in Fig. 4. This is because of low capillary condensation with respect to relative pressure in the pore of the glass thin film. Fig. 5 shows the SEM image of the glass thin film (TEOS:2-PrOH = 1:3). As can be seen, the surface is free from cracks and other deformities. This can be attributed to the decrease of compressive stress during the heat-treatment of the sample. Fig. 6 shows the dependence of conductivity on the relative humidity of the $5P_2O_5$–$95SiO_2$ glass thin film at 30 °C. In addition, it also showed the degree of conductivity of the bulk glass of the same composition for a comparison. The conductivity of the glass thin film at the 80% RH was 2.5×10^{-3} S cm^{-1}. In comparison with the bulk glass, it is understood that the dependence of conductivity on humidity is small. However, the conductivity of the glass thin film as shown in the figure had decreased in com-

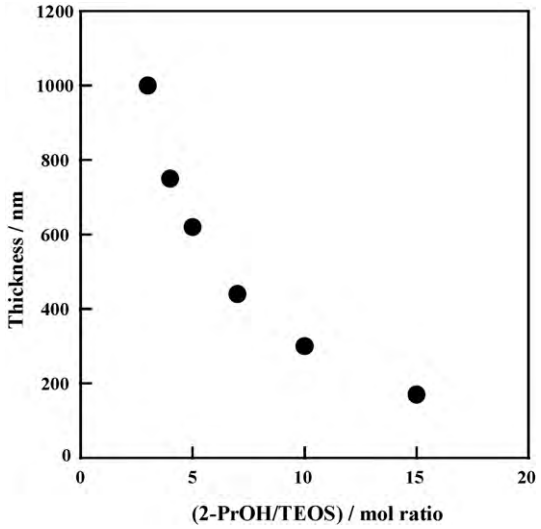

Fig. 2. Relation with mol ratio of 2-PrOH against TEOS and the thickness of glass thin film.

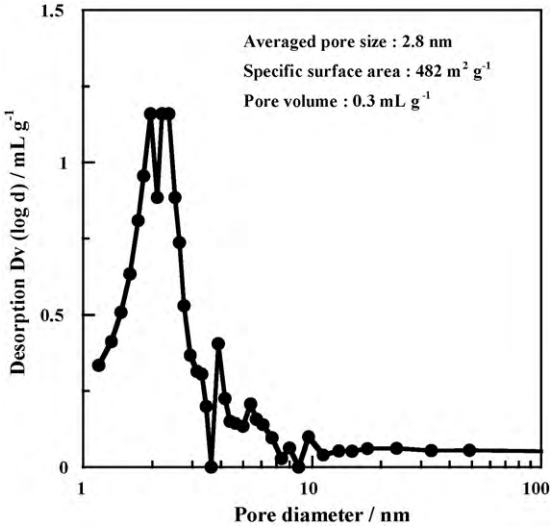

Fig. 3. Pore size distribution of $5P_2O_5$–$95SiO_2$ glass thin film.

Table 1
Pore characteristics of $5P_2O_5$–$95SiO_2$ glass thin film.

Average pore size/nm	Specific surface area/m^2 g^{-1}	Pore volume/mL g^{-1}
2.8	482	0.3

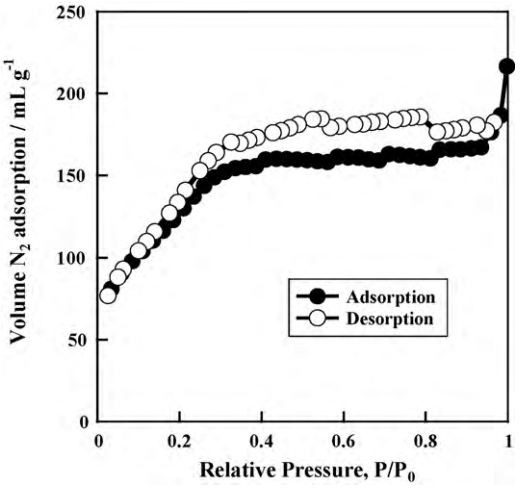

Fig. 4. N_2 adsorption–desorption isotherm of $5P_2O_5$–$95SiO_2$ glass thin film.

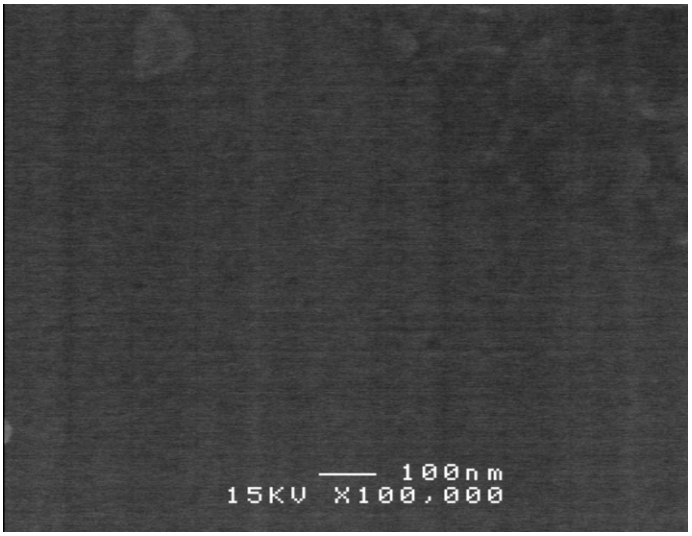

Fig. 5. SEM image of surface of the $5P_2O_5$–$95SiO_2$ glass thin film.

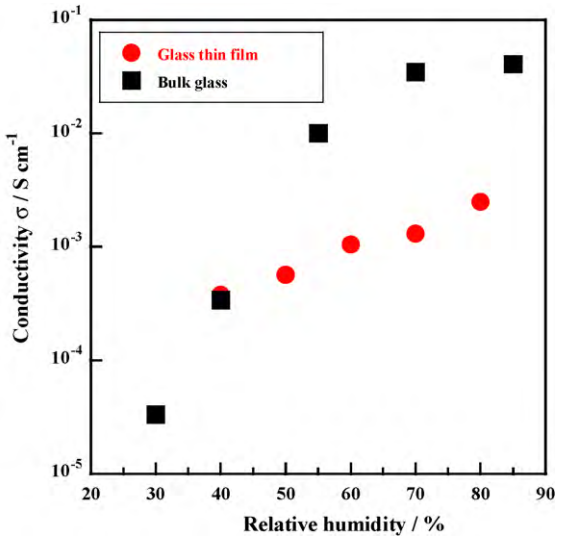

Fig. 6. Relative humidity dependence of the proton conductivity for $5P_2O_5$–$95SiO_2$ glass thin film and bulk glass (30 °C).

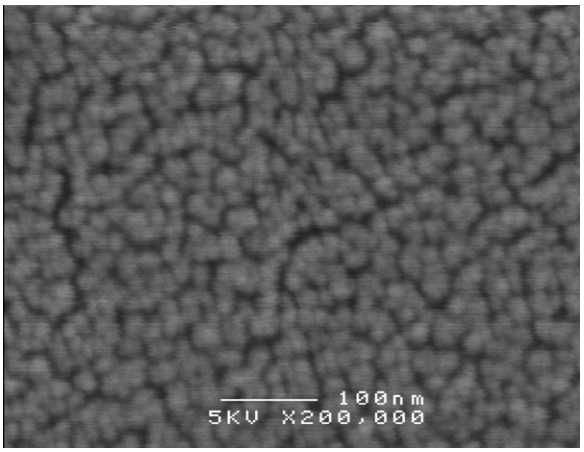

Fig. 7. SEM image of the surface of Pt-sputtered layer.

parison with the bulk glass. In Fig. 7, the surface SEM image of platinum layer is presented. Grain size of the platinum was approximately 20 nm. This size is approximately 5 times greater than that of Pt/C. In Fig. 8, the cross-section SEM image of the prepared membrane electrode assembly (MEA) is presented. The part where the platinum electrode and the glass thin film exfoliated was verified. During the MEA fabrication, the glass thin film and the platinum electrode were heated together. The thermal load and

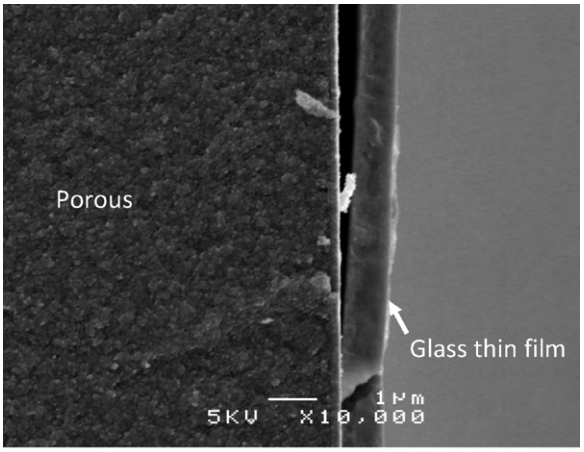

(a) ×10,000

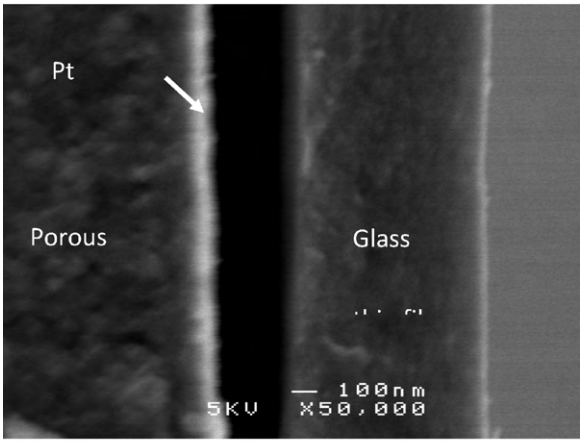

(b) ×50,000

Fig. 8. SEM image of cross-section of MEA (a) ×10,000 and (b) ×50,000.

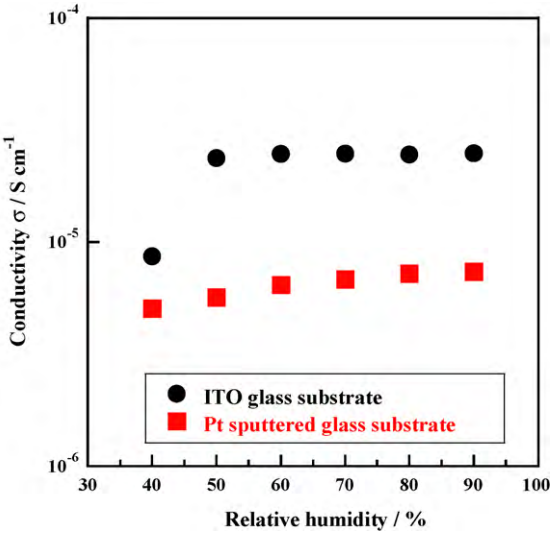

Fig. 9. Relative humidity dependence of the proton conductivity for glass thin film, using different substrates (30 °C).

compressive stress were thought to be responsible for the exfoliation. In Fig. 9, the relative humidity dependence of conductivity of the prepared membrane at 30 °C is presented. It is noted that Fig. 1 shows the preparation of ITO substrate that can be sputtered with Pt layer. The measured conductivity for the ITO-based substrate and the case with Pt layer were 2.49×10^{-5} S cm^{-1} and 7.39×10^{-6} S cm^{-1}, respectively. In comparison, the values were lower than with the $5P_2O_5$–$95SiO_2$ glass thin film. The measured conductivity is thought to be low for samples where adhesion is poor. In addition, as for the conductivity when Pt was used, it was found to be lower in comparison with ITO. We have also studied the characteristics of the fuel cell which uses the glass thin film with MEA (thickness = 1 μm). For a comparison, sample having a film thickness, 0.3 μm is also presented. Fig. 10 shows the time-dependent change of the open circuit voltage of glass thin films. Open circuit voltage at film thickness of 1 μm was measured to be 0.91 V while the film thickness of 0.3 μm was lower. When the film thickness increases, the amount of reaction gas which transmits through the electrolyte will decrease and from this, crossover can be controlled. Fig. 11 shows the potential–current polarization

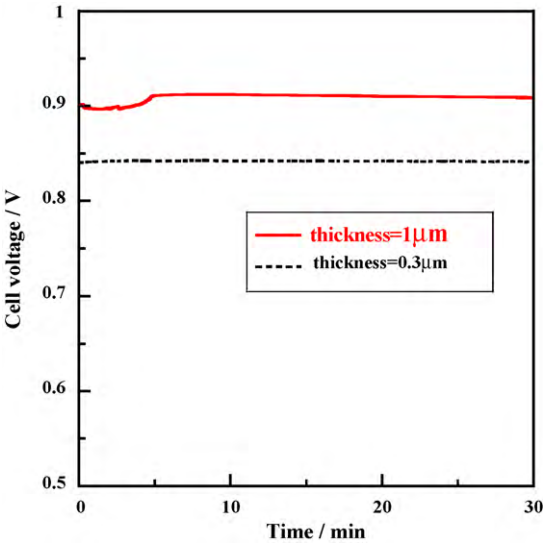

Fig. 10. Change in time of the OCV for fuel cell using glass thin films (R.T., 100%RH).

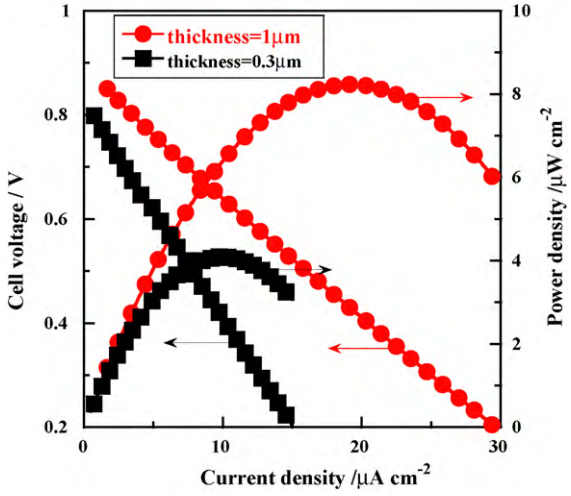

Fig. 11. Potential–current polarization curves of fuel cell glass using glass thin films (R.T., 100%RH).

curves of fuel cells using glass thin films. Maximum output current and power with film thickness 1 μm are 19.1 μA cm^{-2} and 8.2 μW cm^{-2}, respectively, while that of 0.3 μm was lower. When a high open circuit voltage is set, a high load could also be applied. But this is just approximately 1/1000th of the value of the case with bulk glass (1.1 mW cm^{-2}). Fig. 12 shows the impedance spectrum at 0.6 V of MEA. Internal resistance and charge-transfer resistance of 0.3 μm film were 1.9×10^4 and 5×10^3 Ω cm^2, respectively and the total resistance was calculated to be 2.4×10^4 Ω cm^2. As for the bulk glass (film thickness = ~1 mm), the internal resistance and charge-transfer resistance were 15.8 and 5.8 Ω cm^2, respectively. The glass thin film with MEA has reached approximately 1000 times more in terms of its magnitude. The resistance is dictated by the conductivity of the electrolyte and its adhesion with the film, and the electrode used. In comparison with the bulk glass, thickness of the glass thin film is only 1/1000th, making it very thin. By contrast, the conductivity of the glass thin film is greater by 1 order of magnitude than that of the bulk glass. From this, in comparison with the bulk glass, internal resistance of the glass thin film is expected to be reduced by 1/100th. However, the internal resistance of MEA has increased and it is thought that the adhesion of electrolyte and the electrode has caused for this effect. As shown in Fig. 8, the exfoliation of the platinum electrode and the glass thin film can be

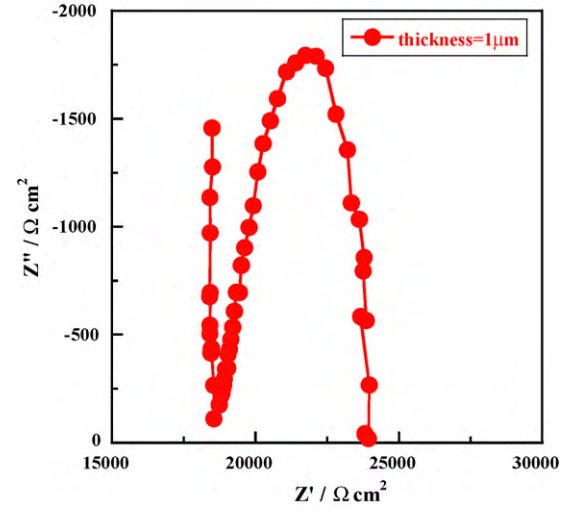

Fig. 12. Impedance spectrum of fuel cell using a glass thin film (R.T., 100%RH).

verified. In order to decrease internal resistance, it is thought that it is necessary to prevent this exfoliation. In addition, the increase in charge-transfer resistance could be due to the three-phase boundary being reduced. This is true for MEA fabricated from MEA bulk glass coupled with Pt/C–Nafion® electrode and sputtered Pt layer.

In the above study, glass thin film (thickness = 1 μm) electrolyte was tested and it showed improvement in the open circuit voltage of the H_2/O_2 fuel cell. The performance of the MEA-assembled fuel cell quality was also evaluated. Below are the findings from this study.

1. Thickness of the glass thin film could be controlled by increasing and decreasing the quantity of 2-PrOH. The ratio TEOS:2-PrOH = 1:3 resulted in a thickness of 1 μm.
2. The conductivity of the glass thin film was 1.5 times lower in comparison with the bulk glass which was $\sim 10^{-3}$ S cm^{-1} and the same conditions, at 80% RH.
3. The electrode has exfoliated from the glass thin film and the poor adhesion of the platinum electrode and the glass thin film was verified.
4. The conductivity of the membrane in vertical direction of the glass thin film was lower with the sputtered Pt layer ($\sim 10^{-6}$ S cm^{-1}) than without Pt layer at 90% RH. It is thought that the poor adhesion of the glass thin film and the platinum electrode resulted into high resistance of the MEA.
5. The open circuit voltage of MEA with 1 μm glass thin film increased to 0.91 V, higher than with 0.3 μm. It is thought that with increase in thickness, crossover of the reaction gas can be decreased.
6. The power output of MEA with 1 μm glass thin film reached approximately 2 times (8.2 μW cm^{-2}) than with the 0.3 μm.
7. As for the internal resistance at 0.6 V of MEA with 1 μm glass thin film and as for charge-transfer resistance, it was measured to be 1.9×10^4 and 5×10^3 Ω cm^2, respectively. Also, it was approximately 1000 times larger in comparison with MEA which used only the bulk glass.

From the above study, the improved open circuit voltage when film thickness of the glass was 1 μm, made clear that in order to obtain a higher output power, it is necessary to make internal resistance and the charge-transfer resistance to be low as much as possible. Adhesion of the sputtered Pt layer and the glass thin film was identified to be directly responsible for the increased internal resistance. It is necessary that in order to make internal resistance decrease, adhesion should be improved so that exfoliation can be prevented. In addition, the sputtered Pt layer also contributed to increased charge-transfer resistance, as the electrode three-phase boundary became small, the reaction at the electrode became unfavorable. In order to make charge-transfer resistance decrease, it is necessary to use catalysts whose three-phase boundary is high. But, it is reported that as for the Pt/C–Nafion® electrode which generally is used as the catalyst for PEMFC, the adhesion of one side and the glass with high three-phase boundary is actually poor. In this work, the electrolyte making use of the Pt/C–Nafion® as the cathode electrode, MEA which is formed with Nafion® membrane as adhesive layer was investigated for improvement in adhesion. In addition, with the purpose of preventing the exfoliation of the Pt layer from the glass thin film, MEA which is formed with TiO_2 layer as an adhesive layer with glass thin film is fabricated. Also, their corresponding fuel cell performance is evaluated.

As for the $5P_2O_5$–$95SiO_2$ sol, the mole ratio was set at TEOS:2-PrOH:H_2O:HCl:Brij®56 = $1:5:5:5 \times 10^{-3}$:0.1.

The synthesis of the TiO_2 sol and its deposition is shown in Fig. 13. Ti $(OC_4H_9)_4$ (or TNBT) was used as the precursor.

First, C_2H_5OH (EtOH) was mixed with TNBT. Next, $(CH_2CH_2OH)_2NH$ (diethanolamine, DEA) as the chelating agent

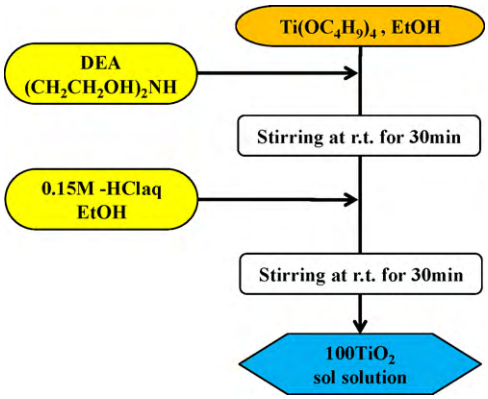

Fig. 13. Flowchart for the sol–gel synthesis of $100TiO_2$.

was added and the solution was stirred vigorously for 30 min at room temperature. After that, EtOH and 0.15 M HCl were added and the solution was further stirred for another 30 min in order to produce the $100TiO_2$ sol. Mole ratio of the final reactant (mol%) was TNBT:DEA:EtOH:H_2O:HCl = 1:1:29.6:1:1.

3.1. Electrode preparation

For the electrodes, those used for polymer electrolyte fuel cells were generally prepared from the electrode slurry. The preparation method is as follows. Nafion® solution (5 wt.%, 1.0 g, Aldrich) with PTFE suspension (polytetrafluoroethylene; 10 wt.%, 0.4 g, Aldrich) were agitated lightly. To this solution, platinum support carbon catalyst (Pt/C; 0.1 g) was added for 1 h ultrasonic dispersion. After that, ethanol aqueous solution (40 vol% and 1.0 g) was added and followed with another 3 h of ultrasonic dispersion. The obtained solution was designated as the electrode slurry. The synthetic process of this electrode slurry is shown in Fig. 14. This solution was noted to have high catalyst activity with its high specific surface area.

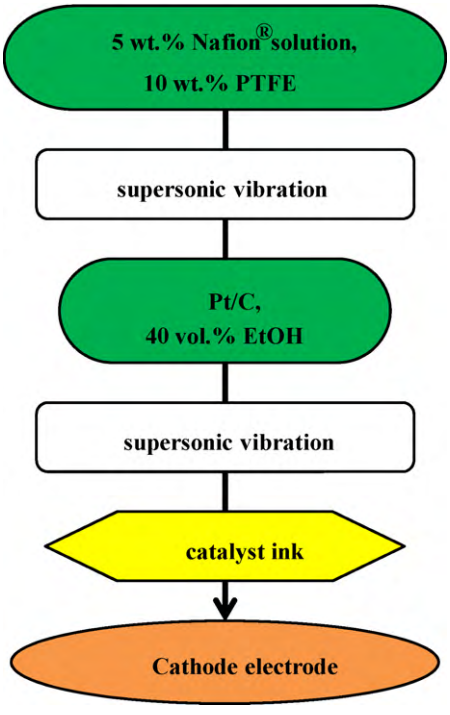

Fig. 14. Flowchart of the synthesis of catalyst ink.

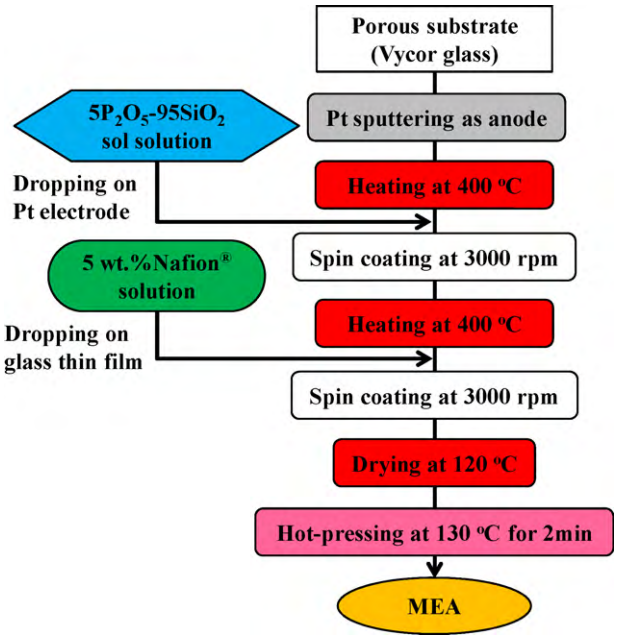

Fig. 15. Flowchart for the fabrication of the MEA using Nafion film as an intermediate layer.

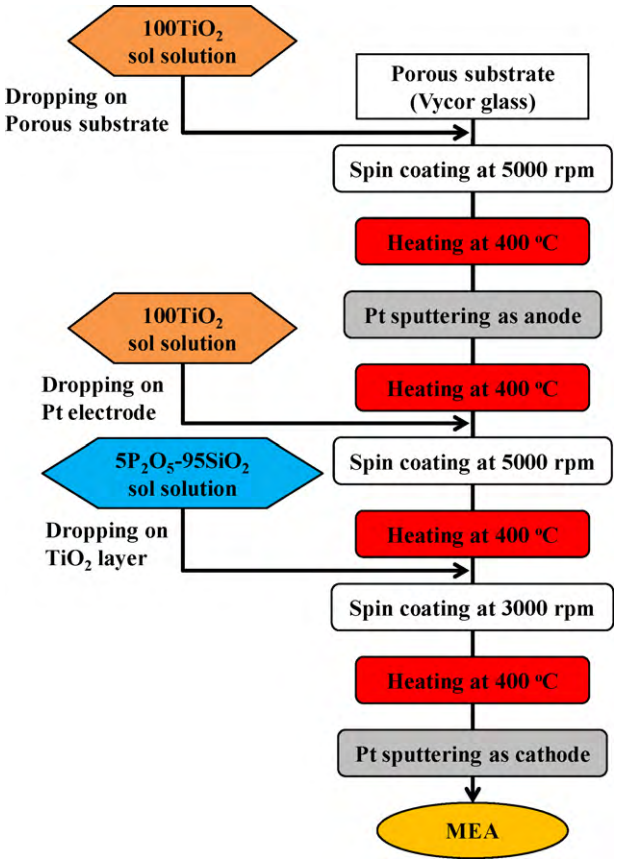

Fig. 16. Flowchart for the fabrication of the MEA using TiO_2 as an intermediate layer.

3.2. The production of MEA

3.2.1. The cathode electrode – MEA made with Nafion® membrane between the glass thin film

First, the anode electrode was made by using one side of the Vycor glass base plate which was mirror-polished in which Pt was deposited by a sputtering machine (Sanyuu, Co., Electronic SC-701 type) for 3 min. After that, heated treatment at 400 °C followed. Then, the $5P_2O_5$–$95SiO_2$ precursor solution, after 1 h of aging, was spin-coated on the Vycor glass substrate at 3000 rpm. Next, it was heated at 400 °C. After that, the Nafion® solution (5 wt.%, Aldrich) was also spin-coated on the glass thin film surface at 3000 rpm and then dried at 120 °C. The carbon paper with catalyst slurry (0.9 cm × 0.9 cm) was then placed on the Nafion® membrane surface. And, making use of small-sized thermal press machine (Azuwan Corporation, AH-2003), the assembly was hot-pressed for 2 min at 130 °C and 2 MPa in order to bond the cathode electrode and the Nafion® membrane. To prevent any damage, the sample was placed between the Teflon sheet and rubber sheet. The lead wire was installed with silver paste (as an adhesive) on the anode and cathode sides for the electron microscope (Nisshin EM (Inc.), Sillbest P255). The preparation procedure and schematics of this MEA are shown in Figs. 15 and 17(a), respectively.

3.2.2. The anode electrode – MEA made with TiO_2 layer between the glass thin film

First, using the $100TiO_2$ precursor solution, the mirror-polished side of the Vycor glass baseplate was spin-coated with TiO_2 layer at 5000 rpm, following heat-treatment at 400 °C. Using the sputtering machine with respect to TiO_2 layer, the Pt layer was deposited for 3 min as anode, followed by heat-treatment at 400 °C. Then, with respect to platinum layer, the $100TiO_2$ was again spin-coated at 5000 rpm and then heat-treated at 400 °C. Next, the prepared $5P_2O_5$–$95SiO_2$ sol was spin-coated on top of the previous layer at 3000 rpm, following heat-treatment at 400 °C. Then a final Pt sputtering (as cathode) was made with the same sputtering parameters. The cathode electrode (0.9 cm × 0.9 cm), the masking point to the glass thin film surface was sputtered with Pt for 2 min. The lead wire was installed on the anode and cathode by using silver paste as an adhesive. The production procedure and schematics of this MEA are shown in Figs. 16 and 17(b), respectively.

3.3. Characteristics of the TiO_2 layer

3.3.1. Pore quality

In Fig. 18, the pore size distribution of the TiO_2 layer is shown. Table 2 shows the TiO_2 layer's average pore size, specific surface area and pore volume. The specific surface area, and pore volume were smaller than with the result of the $5P_2O_5$–$95SiO_2$ glass thin film as shown in Table 1.

3.3.2. Conductivity of the TiO_2 layer

Fig. 19 shows the relative humidity dependence of the proton conductivity for TiO_2 layer, measured using interdigital electrode (30 °C). The degree of conductivity measured for the TiO_2 layer at 90% RH is 2.2×10^{-4} S cm^{-1}. As for TiO_2 which was produced by sol–gel method, the conductivity is low in comparison with the $5P_2O_5$–$95SiO_2$ glass thin film.

3.3.3. The adhesion of the fabricated MEA

In Fig. 20, the cross-section SEM image of MEA showing the TiO_2 layer between the anode electrode and the glass thin film is presented. As can be seen, there is no exfoliation of electrolyte from the platinum electrode in comparison with when the TiO_2 layer is not used (as shown in Fig. 8 of above section). The thermal load and the compressed stress at the Pt-sputtered layer can be decreased by the TiO_2 layer and adhesion is promoted. The TiO_2 layer prepared by sol–gel method was confirmed to be an effective adhesive layer. In addition, when there is no Nafion® membrane, the electrode peels off. Meanwhile, no peeling off occurred with the cathode electrode when Nafion® membrane as an adhesive layer was used in

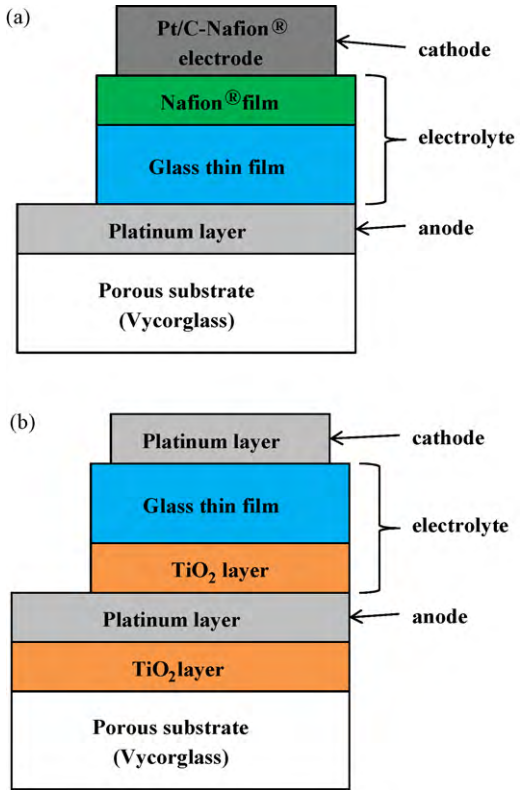

Fig. 17. Scheme of the MEA using (a) Nafion film and (b) TiO_2 as an intermediate layer.

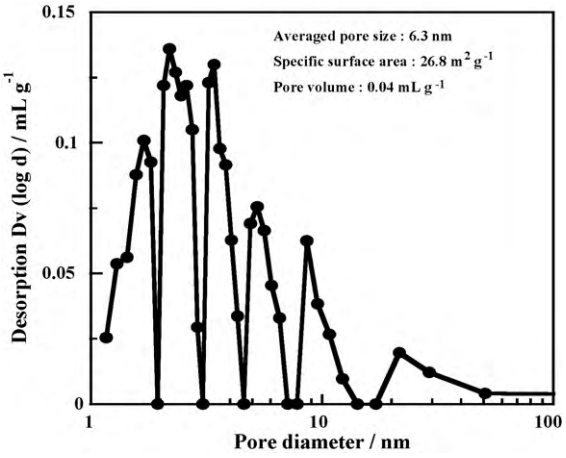

Fig. 18. Pore size distribution of TiO_2 layer.

the MEA. Fig. 21 presents the relative humidity dependence of conductivity of membrane in vertical direction, at 30 °C. The degree of conductivity at 90% RH of samples without adhesive layer, with Nafion® membrane and TiO_2 layer were 2.57×10^{-6}, 2.57×10^{-6} and 6.83×10^{-6} S cm^{-1}, respectively. When the Nafion® membrane is designated as adhesive layer, it was same in comparison with the conductivity of samples without it. When TiO_2 layer is designated as adhesive layer, it improved the conductivity more than 2.5 times

Table 2
Pore characteristics of TiO_2 layer.

Average pore size/nm	Specific surface area/m^2 g^{-1}	Pore volume/mL g^{-1}
6.3	26.8	0.04

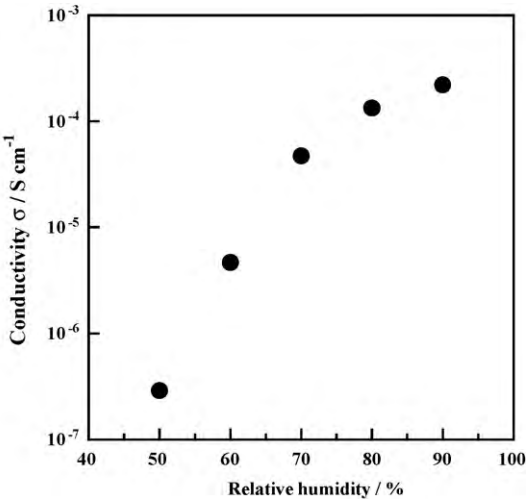

Fig. 19. Relative humidity dependence of the peculiar proton conductivity for TiO_2 layer, measured using interdigital electrode (30 °C).

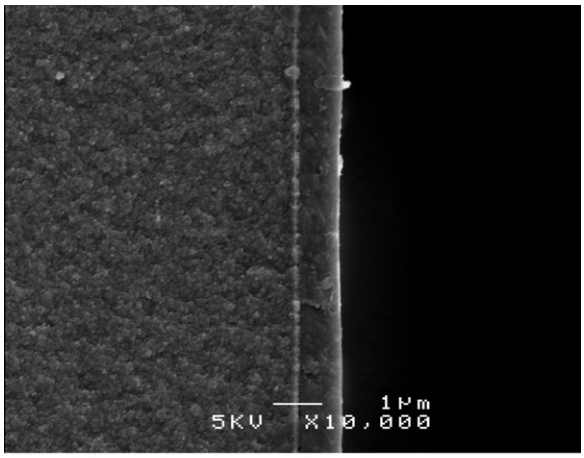

(a) ×10,000

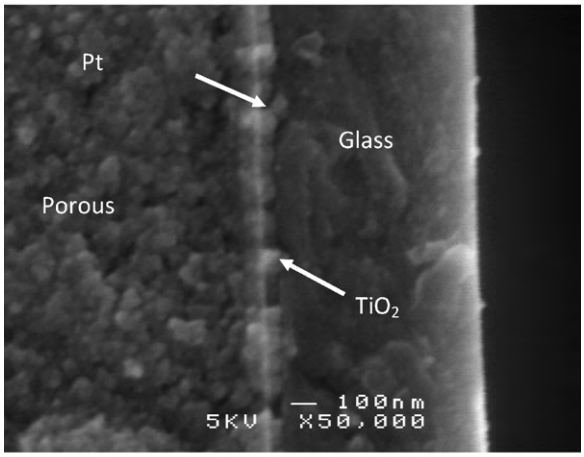

(b) ×50,000

Fig. 20. SEM image of the cross-section of the MEA using TiO_2 layer as an intermediate layer (a) ×10,000 and (b) ×50,000.

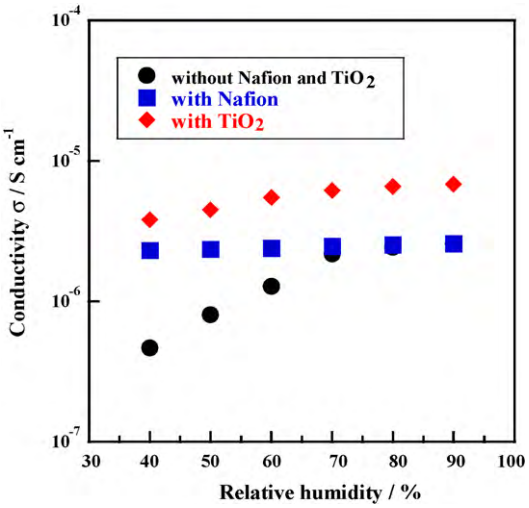

Fig. 21. Relative humidity dependence of the conductivity for the prepared MEA (30 °C).

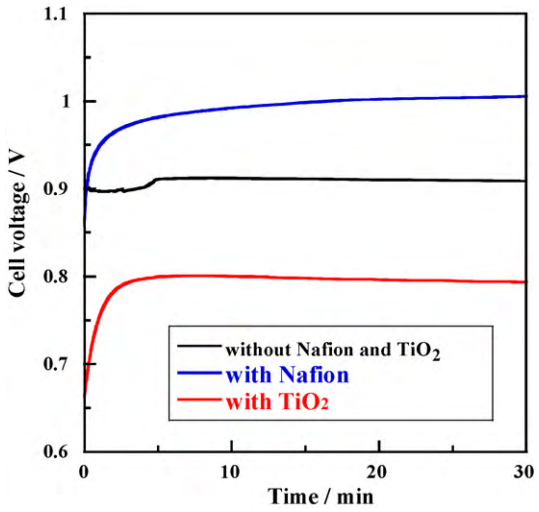

Fig. 23. Change in time of open circuit voltages for fuel cells using prepared MEAs (R.T., 100%RH).

at 90% RH. As understood from the SEM image in Fig. 20, adhesion of the electrode and electrolyte increased, thereby decreasing the resistance in the boundary and improving the conductivity. Fig. 22 shows the change in conductivity with the film thickness of the TiO_2 layer at 90% RH and 30 °C. The line in the figure represents the degree of conductivity at 90% RH, when TiO_2 layer is not used as adhesive layer. As film thickness becomes thin to 300–100 nm, degree of conductivity reached high value. As shown in figure, the membrane resistance of TiO_2 increases because 1 column is low as for TiO_2 specific degree of conductivity in comparison with the glass thin film. But, the degree of conductivity equality or reached low value is at 100 nm or less. The effective film thickness, from this, is 100 nm as an adhesive layer. The film thickness of the sample was measured by a surface roughness meter. Here, the glass thin film (thickness = 1.5 mm) of MEA was used as the Nafion® membrane (thickness = 200 nm) for adhesive layer. In addition, the glass thin film of MEA which uses TiO_2 for adhesive layer and film thickness of TiO_2 layer, were 620 and 100 nm, respectively. Fig. 23 shows the time-dependent change of the open circuit voltage of the fabricated MEA. When adhesive layer is not used, when Nafion® membrane and when TiO_2 layer is used as adhesive layers, the open circuit voltages were 0.91 V, 1.01 V and 0.81 V, respectively. As the film thickness of the electrolyte of MEA changes, the cross leak of the extent reaction gas through film also changes. When the Nafion® membrane is used as adhesive layer and with the catalyst slurry which is produced for the cathode electrode from Pt/C, voltage decreased in comparison with Pt-sputtered layer usage. This is one of the primary factors where one can obtain high open circuit voltage. Fig. 24 shows the impedance spectra at 0.6 V of the fabricated MEA. The internal resistance and charge-transfer resistance when adhesive layer is not used are $1.9 \times 10^4\ \Omega\,cm^2$ and $5 \times 10^3\ \Omega\,cm^2$, respectively. When Nafion® membrane is used for adhesive layer these values are $4.9 \times 10^3\ \Omega\,cm^2$ and $5.0 \times 10^3\ \Omega\,cm^2$; and when TiO_2 layer is used they are $1.7 \times 10^3\ \Omega\,cm^2$ and $1.9 \times 10^4\ \Omega\,cm^2$, respectively. The internal resistance decreased when Nafion® membrane or TiO_2 layers are used as adhesive layers. When the Nafion® membrane is used for adhesive layer, the adhesion increased in comparison with when the Nafion® membrane is not used by bonding with the cathode electrode, and the Nafion® membrane with hot pressing had caused internal resistance to decrease. But, decrease of charge-transfer resistance was not seen. This is because the platinum electrode was used for the anode electrode. When TiO_2 layer is used for adhesive layer, as shown in Fig. 8, adhesion with the platinum electrode and the glass thin film resulted in the decrease in internal resistance by preventing exfoliation. But on the other hand, charge-transfer resistance increased. The three-phase circuit boundary in the anode electrode of the fabricated MEA is thought

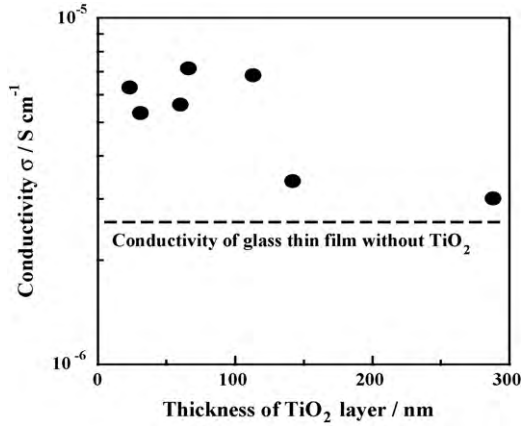

Fig. 22. Relation with thickness of TiO_2 layer and the conductivity (30 °C, 90%RH).

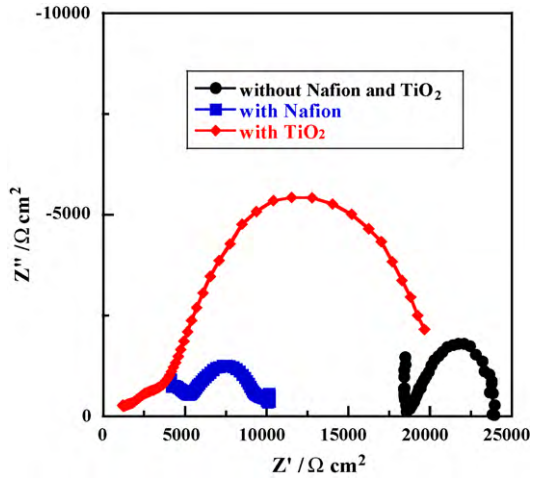

Fig. 24. Impedance spectra at 0.6 V of fuel cells using prepared MEAs (R.T., 100%RH).

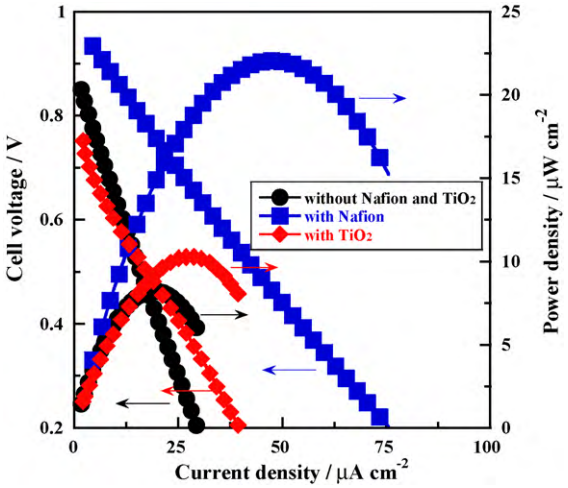

Fig. 25. Potential–current polarization curves of fuel cells using prepared MEAs (R.T., 100%RH).

to form only to the boundary part of anode electrode and electrolyte. Because with TiO_2 layer and platinum electrode and the reaction gas whose degree of conductivity is low in comparison with the $5P_2O_5$–$95SiO_2$ glass thin film and with the three-phase circuit boundary formed, it is thought that charge-transfer resistance is increased. It is understood that the overall resistance of the whole MEA decreases, with the Nafion® membrane and TiO_2 layer as adhesive layers. In Fig. 25, the current–voltage characteristics of the fabricated MEA are shown. The maximum power output when no adhesive layer was used was 8.2 μW cm^{-2} at 19.1 μA cm^{-2}. When the Nafion® membrane was used it is 22.1 μW cm^{-2} at 47.6 μA cm^{-2} and when TiO_2 layer was used these values were 10 μW cm^{-2} at 27.7 μA cm^{-2}. The output is improved by using an adhesive layer. As shown in figure, the decrease in resistance of the whole MEA is notable. But, only values where output is low were obtained. It is thought that there is a problem in the electrode. The value was approximately 5 times higher in comparison with one generally used PEFC with of Pt/C of which 20 nm grain size of the platinum layer was used as the anode and cathode and is considerably large. From this, the specific surface of Pt turned to be small and that catalyst activity would be low also. In addition, not only the cathode electrode, it is also necessary to increase three-phase circuit boundary in the anode electrode to obtain high power and current densities. The electrode adhesion in the electrolyte was improved by forming adhesive layer as indicated in the above section. It is understood from there, which the resistance of MEA decreases. But, the output is still low value. As for the platinum sputtered layer which it has been verified to have low power output, as an anode as shown in Fig. 7, platinum grain size ~20 nm is approximately 5 times more in comparison with Pt/C which is used as the catalyst for PEFC. Because grain size is large, in addition to the small specific surface area, catalyst activity decreased. In addition, with the platinum sputtered layer it is thought that formation of three-phase boundary is limited. From these things it can be said that, it is important to use the catalyst whose three-phase boundary is high even in the anode electrode. But, when the electrode which uses Pt/C on the substrate is used, formation of the glass thin film is difficult. As it is lacking in heat resistance, it is difficult to produce MEA with the former. So, it is necessary to examine the production method of new MEA.

In order to solve this problem, the fabrication of MEA which makes both electrodes on the identical surface of electrolyte was tried. And, the fuel cell performance of the MEA was evaluated. The substrate used for conductivity measurement and for current/voltage characteristics measurement was a slide glass (MATSUNAMI Company). The conductivity measurement was made in the thermo-hygrostat (the ESPEC corporation make, SH-221) after temperature and humidity has become fixed (approximately 1 h). As for measurement temperature, it was 30 °C, as for relative humidity, it is changed within 40–80% RH.

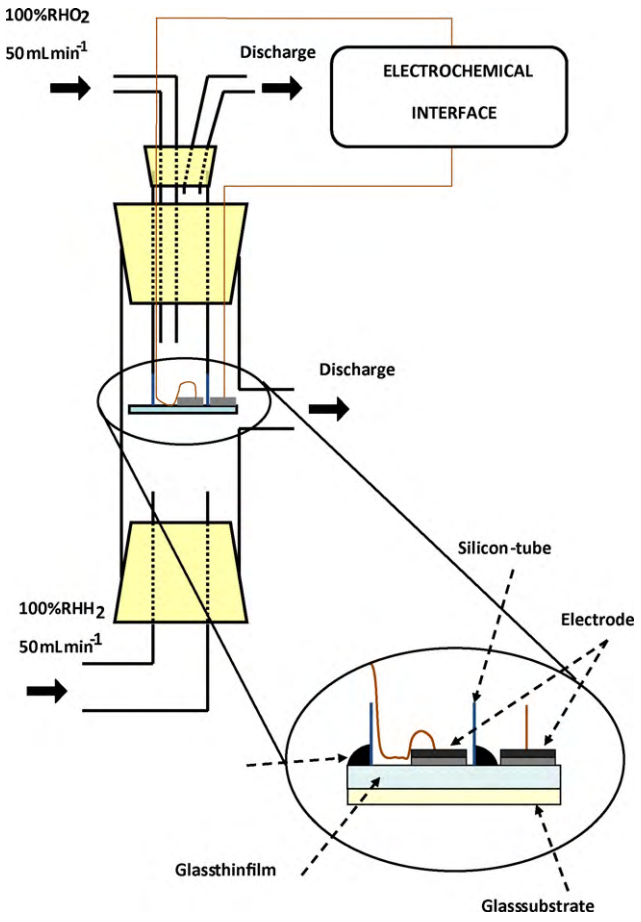

Fig. 26. Hydrogen–oxygen fuel cell mechanism.

3.4. Fabrication of MEA

First, the produced $5P_2O_5$–$95SiO_2$ precursor solution after 1 h aging, was coated on slide glass substrate by spin coating at 2000 rpm, and then followed by heating in the furnace at 400 °C. The carbon paper with the catalyst slurry which was produced, the anode and the cathode electrodes were installed on the glass thin film surface. The lead wire was installed with silver paste as an adhesive on these electrodes. The device which is used for the measurement of current/voltage characteristics is shown in Fig. 26. The lead wire was installed on both electrodes with the silver paste as an adhesive. With the adhesive ([semedain] (Inc.) and SUPER X clearing) of silicon type, the silicon tube supports were attached on thin film and after 24 h drying; it was installed in the hydrogen–oxygen electric battery cell. On anode electrode side, the H_2 gas with flow rate 50 mL min^{-1} while a flow of 50 mL min^{-1} of circulated O_2 gas on cathode electrode side was allowed. Voltage and electric current between the terminals were measured making use of Solartron 1287 types ELECTROCHEMICAL INTERFACE.

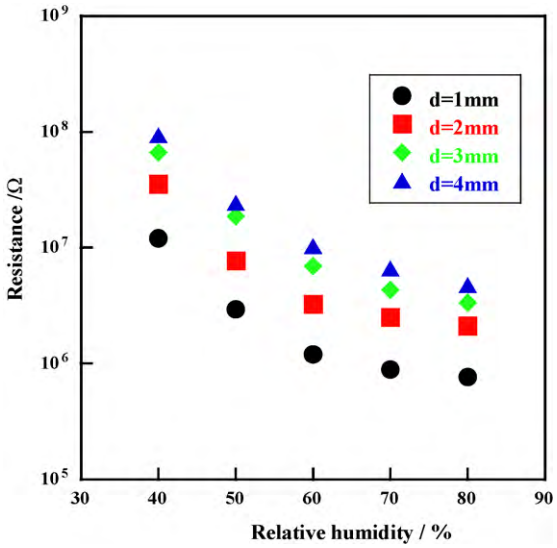

Fig. 27. Relative humidity dependence of resistance when the distance *d* between the electrodes is changed (electrode length = 13 mm, electrode width = 5 mm, film thickness, *t* = 250 nm of the glass thin film at 30 °C).

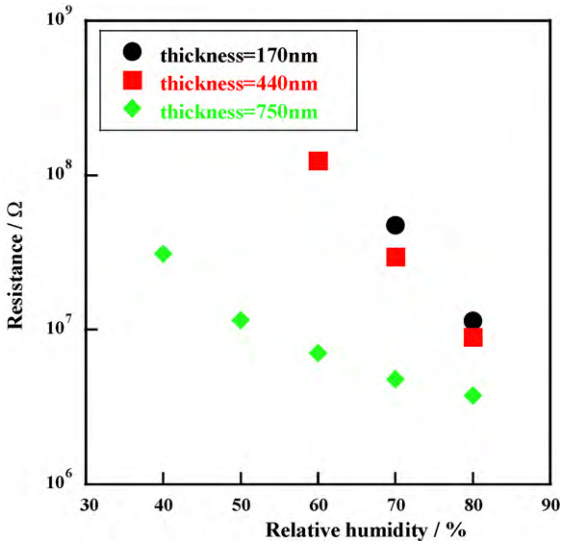

Fig. 28. Film thickness *t* the relative humidity dependency of resistance when the film thickness *t* is changed (electrode length = 13 mm, electrode width = 5 mm, distance *d* = 4 mm between the electrodes at 30 °C).

3.5. Resistance evaluation

3.5.1. When the distance between the electrodes is changed

The relative humidity dependence of resistance at 30 °C when the distance *d* between the electrodes was changed is shown in Fig. 27. The value of resistance at 80% RH when distance d between the electrodes is 1,2, 3 and 4 mm was 7.7×10^5, 2.1×10^6, 3.4×10^6 and 4.7×10^6 Ω, respectively. As distance between the electrodes increases, the resistance also increases. It is understood that the decrease in resistance is possible, from the result, by making the distance between the electrodes short. In the identical face form (referring to the way the assembly was made), the distance between the electrodes is suitable for film thickness.

3.5.2. When the film thickness of the glass thin film is changed

The relative humidity dependence of resistance at 30 °C when the film thickness *t* of the glass thin film changed is shown in Fig. 28. The value of resistance at 80% RH, when film thickness *t* was 750, 440 and 170 nm was 3.7×10^6, 8.9×10^6 and 1.1×10^7 Ω, respectively. As film thickness increases, resistance decreases. In the identical face form (referring to the way the assembly was made), the electrode area and electrode length is thought to be suitable to the cross-sectional area part of the glass thin film.

3.5.3. When the electrode width is changed

The relative humidity dependence of resistance at 30 °C when the electrode width changed is shown in Fig. 29. The value of resistance at 80% RH when electrode width is 2, 5 and 8 mm was 9.3×10^5, 1.1×10^6 and 2.0×10^6 Ω, respectively. As electrode width becomes smaller, resistance decreases. In the identical face form (referring to the way the assembly was made), conduction route of the proton was thought as, distance $d + 2 \times$ electrode width between the electrodes. Because conduction route becomes shorter, due to the fact that electrode width becomes smaller, the resistance decreased.

3.6. Fuel cell performance

In Fig. 30, the impedance spectrum at 0.6 V of the fabricated MEA is shown. When electrode width is 4 or 9 mm, internal resistance values were about 0.37 and 1.7 Ω cm^2 while for charge-transfer resistance the values were 0.81 and 0.95 Ω cm^2, respectively. In comparison with the bulk glass, internal resistance and charge-transfer resistance decreased. As for the bulk glass, the electrolytic surface is not even, the contact area of the electrode is not sufficient. But, the glass thin film surface is thought to be even and the contact area of the electrode increases. In addition, the internal resistance was decreased by making electrode width narrow. As for this, when the electrode is arranged on the surface, conduction route of the proton becomes short, due to the fact that resistance decreases. In Fig. 31, the electric current–voltage characteristics of the fabricated MEA are shown. When electrode width is 4 or 9 mm, the current and power output values were 147.1 mA cm^2 and 73.8 mW cm^2; and 68.2 mA cm^2 and 27.2 mW cm^2, respectively. It is thought that catalyst reaction efficiency in three-phase boundary improved and higher outputs can be obtained with the electrodes used. In addition, high output value was observed when electrode width is small. This corresponds with the fact that internal resistance is decreased.

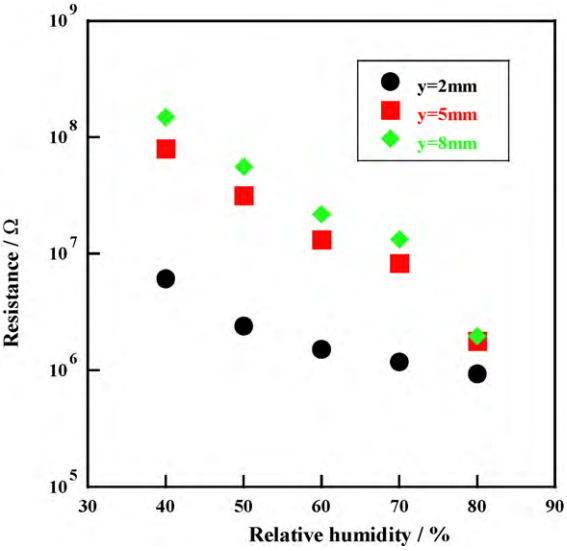

Fig. 29. The relative humidity dependence of resistance when electrode width is changed (electrode length = 13 mm, distance = 1 mm between the electrodes, film thickness *t* = 750 nm of the glass thin film at 30 °C).

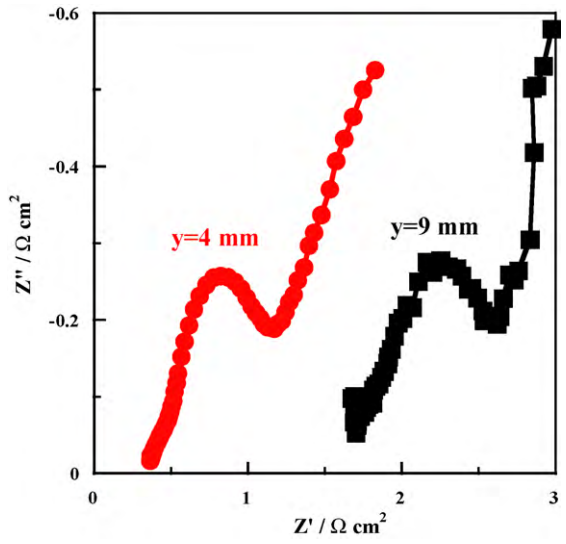

Fig. 30. The impedance spectrum at 0.6 V of the identical face form MEA (distance = 1 between the electrodes mm, film thickness t = 750 nm of the glass thin film, electrode length = 9 mm, room temperature and 100% RH).

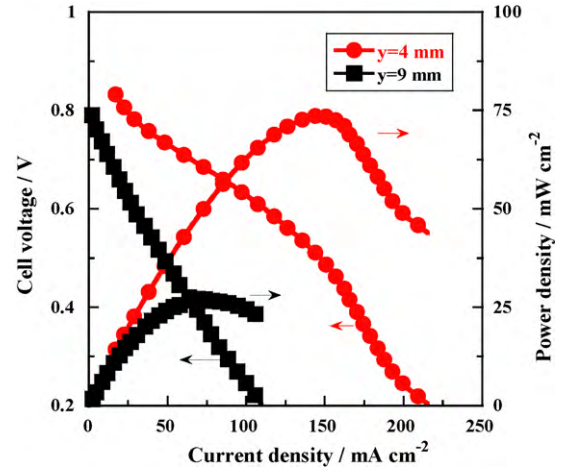

Fig. 31. Electric current–voltage characteristic of the identical face form MEA (distance d = 1 mm between electrodes, film thickness t = 750 nm of glass thin film, electrode length = 9 mm, room temperature and 100% RH).

4. Conclusions

In this study, the goal of decreasing the resistance of the whole MEA by the use of TiO_2 layer and Nafion® membrane as adhesive layer was realized. The facts in this work which became clear are shown below.

1. TiO_2 layer showed the degree of conductivity of 2.2×10^{-4} S cm^{-1} at 30 °C and 90% RH.
2. By the fact that bonding was promoted with hot pressing, cathode peeling off was prevented with Nafion® membrane as an adhesive layer. In addition, through TiO_2 layer, it stuck to MEA when TiO_2 layer was used as adhesive layer; with the platinum electrode and the glass thin film, exfoliation was not happened.
3. The degree of conductivity in the membrane vertical direction of the sample with TiO_2 layer was improved approximately 2.5 times in comparison with when TiO_2 layer is not used.
4. When TiO_2 layer was used as adhesive layer, 100 nm thickness was determined to be the optimum.
5. The internal resistance of MEA was decreased with the Nafion® membrane or TiO_2 layer as adhesive layer, the value was 4.9×10^3 Ω cm^2, in comparison with 1.7×10^3 Ω cm^2 when no adhesive layer was used. Because adhesion between electrolyte and electrodes increases, the resistance of the whole MEA decreased together.
6. As for the maximum power output of MEA which uses the Nafion® membrane or TiO_2 layer as adhesive layer, the value was 22.1 μW cm^{-2} and for the case without adhesive layer, the value was only 10.3 μW cm^{-2}. In addition, it is thought that when it uses the Nafion® membrane as adhesive layer, the increase in three-phase circuit boundary of cathode electrode side had contributed to the improvement of output.
7. As for the charge-transfer resistance of MEA, around 5.0×10^3 Ω cm^2, which uses the Nafion® membrane for adhesive layer, the change was not seen in comparison with when it was not used. In addition, in the case of TiO_2 layer, with a value about 1.9×10^4 Ω cm^2, it increased in comparison with when no TiO_2 layer was used. Together, the Pt-sputtered layer as an anode electrode, it is thought that the limited formation of three-phase circuit boundary in this electrode has had an influence on the increase of charge-transfer resistance.

   The fabrication of the identical face form MEA which uses the glass thin film and the evaluation on its fuel cell performance was studied.

   The resistance could be decreased by making the distance between the electrodes smaller. The distance between the electrodes is related to film thickness.
8. The resistance could be decreased by increasing the film thickness, t. In the identical face form, the electrode area and electrode length were suitable to the cross-sectional area part of the glass thin film.
9. The resistance could be decreased by making electrode width smaller. In the identical face form, conduction route of the proton (distance $d + 2 \times$ electrode width between the electrodes) became short, due to the fact that electrode width became short.
10. The low internal resistance in the time of fuel cell operation occurred when electrode width is small.
11. The power output of the fabricated MEA 73.8 mW cm^{-2} is a high value. The three-phase boundary is high in the anode and cathode, along with that the catalyst efficiency improvement.

Acknowledgment

The authors are grateful to the New Energy and Industrial Technology Development Organization (NEDO), Japan for financial support.

References

[1] M. Nogami, H. Matsushita, Y. Goto, T. Kasuga, Adv. Mater. 12 (18) (2000) 1370–1372.
[2] T. Uma, M. Nogami, Chem. Mater. 19 (15) (2007) 3604–3610.
[3] M. Nagai, K. Kobayashi, Y. Nakajima, Solid State Ionics 136–137 (2000) 249–254.
[4] S.J. Huang, H.K. Lee, W.H. Kang, Bull. Korean Chem. Soc. 26 (2) (2005) 241–247.
[5] T. Uma, S. Izuhara, M. Nogami, J. Eur. Ceram. Soc. 26 (12) (2006) 2365–2372.
[6] T. Uma, A. Nakao, M. Nogami, Mater. Res. Bull. 41 (4) (2006) 817–824.
[7] M. Aparicio, L.C. Klein, J. Sol–Gel Sci. Technol. 28 (2) (2003) 199–204.
[8] Ph. Colomban (Ed.), Proton Conductors: Solids, Membranes and Gels—Materials and Devices, Cambridge Univ. Press, Cambridge, 1992.
[9] U. Lavrencic Stranger, N. Groselj, B. Orel, A. Schmitz, Ph. Columbin, Solid State Ionics 145 (2001) p.109–118.
[10] A. Horky, N.P. Kherani, G. Xu, J. Electrochem. Soc. 150 (9) (2003) A1219–A1224.
[11] M. Uchida, Y. Aoyama, Y. Sugawara, H. Ohara, A. Ohta, J. Electrochem. Soc. 145 (1998) 3708–3713.
[12] P. Colomban, Proton conductors, Chemistry of Solid State Materials, Cambridge University press, Cambridge, London, 1992, p. 2.
[13] Y. Daiko, T. Kasuga, M. Nogami, Chem. Mater. 14 (2002) 4624–4627.
[14] Y. Daiko, T. Kasuga, M. Nogami, J. Sol–Gel Sci. Technol. 26 (2003) 1041–1044.
[15] M. Nogami, R. Nagao, K. Makita, Y. Abe, Appl. Phys. Lett. 71 (10) (1997) 1323–1325.
[16] Y. Daiko, T. Akai, T. Kasuga, M. Nogami, J. Ceram. Soc. Jpn. 109 (10) (2001) 815–817.